2010 IEEE International Conference on Robotics and Automation
Anchorage Convention District
May 3-8, 2010, Anchorage, Alaska, USA

Towards Accurate Motion Compensation in Surgical Robotics

Andreas Tobergte, Florian A. Fröhlich, Mihai Pomarlan, and Gerd Hirzinger

Abstract— **This paper proposes a method for accurate robotic motion compensation of a freely moving target object. This approaches a typical problem in medical scenarios, where a robotic system needs to compensate physiological movements of a target region related to the patient. An optical tracking system measures the poses of the robot's end-effector and the moving target. The task is to track the target with the robot in a desired relative pose. Arbitrary motion in 6 DoF is covered. The position controller of the medical light-weight robot MIRO is enhanced by a Cartesian displacement observer. The proposed observer feedback preserves the dynamics of the robot, while achieving high accuracy in task space. The target object is equipped with an inertial measurement unit in addition to tracking markers. Target sensor data is fused by an extended Kalman filter in a tightly coupled approach. The robot control and the target tracking in the task space aim to combine accuracy, dynamic performance and robustness to marker occlusions. The algorithms are verified with the DLR MIRO, an experimental target platform, and a commercial tracking system. The experiments demonstrate rapid convergence to desired Cartesian poses and good dynamic tracking performance even at higher target motion speed.**

Fig. 1. The MIRO, a versatile medical light-weight robot developed at the German Aerospace Center (DLR); An experimental platform with tracking markers and an inertial measurement unit; An optical tracking system

I. INTRODUCTION

In modern operating rooms optical tracking systems (OTS) are widely used for navigation and are the state of art in accuracy. In neurosurgery, e.g. surgeons navigate hand held tools equipped with reflecting marker balls while looking at a monitor visualizing the tool in a virtual patient. The 3D data of patients is preoperatively recorded by computer tomography (CT) or magnetic resonance imaging (MRI). The markers of the tracking system are registered with respect to the 3D data. After this preoperative scanning, planning and registration phase, the tool and the patient can be monitored intraoperatively in one reference system, which is defined by the optical tracking system. The introduction of robots into the operating room as a assistance device for surgeons demands the integration of the robot in this environment. We developed an application for placement of pedicle screws with the Kinemedic, a versatile medical light-weight robot [12], a predecessor of the MIRO (see fig. 1). Tracking markers are attached to the robot and the control loop is closed by the tracking system. However, compensation of motion of the vertebra is not the focus, it rather aims to achieve static accuracy only. A similar application is addressed in [3], were a pedicle screw is inserted in spinal fusion. Tracking markers are attached to the operating area, but not to the robot. The planned trajectory is modified online with the tracking data and sent to the robot controller.

In this paper, we address the more abstract task of controlling a robot with respect to a navigated object in the task space, which is defined by a tracking system or a similar external sensor. This represents a typical medical scenario, as described above for pedicle screw placement or e.g. laser osteotomy on the sternum. The task is divided into two subtasks: (1) Accurate and fast control of the robot in the task space. (2) Tracking of an object, which is fixed to the patient. The task is executed without any assumptions regarding periodicity of physiological motion and with 6 DoF in the task space. The experimental system is implemented with the medical light-weight robot MIRO [19]. The MIRO is kinematically redundant with a joint configuration similar to the human arm. Torques are measured in all seven DoF in addition to position sensing for compliant and position control mode. A full-state feedback position controller for the MIRO with coupled, flexible joints is presented in [10]. The robot control enhanced with the tracking system aims to: (a) increase the accuracy in the task space, (b) preserve the good dynamics of the existing position controller, as well as the robustness with respect to marker occlusions. The tracked object is an experimental platform with markers for the OTS and an inertial measurement unit (IMU), measuring 3 DoF acceleration and 3 DoF angular velocity. The combined OTS/IMU system aims to: (a) increase the robustness with respect to marker occlusions, (b) compensate for delay of

All authors are affiliated with the Institute of Robotics and Mechatronics, German Aerospace (DLR), 82234 Wessling, Germany andreas.tobergte@dlr.de

the OTS, (c) reduce noise [18]. For both subtasks the combination of accuracy and dynamic performance are key issues.

In section II a review of accurate robot control and object tracking with multiple sensors is given. In the following sections III, and IV, our approaches for the control task and the object tracking are presented, respectively. Experimental results of the task space controller and the combined motion compensation with OTS/IMU are given in section V. Section VI concludes the paper and gives an outlook on future work.

II. State of the art

In this section an overview of recent works related to the two subtasks accurate robot control and multi sensor object tracking is given.

A. Accurate Robot control

This section describes the usage of visual tracking combined with robotics as it is predominantly applied in industrial and medical scenarios. With increasing processing power optical sensors are very suitable for contact free measurements in complex environments. There is a wide range of algorithms and measurement systems available, varying from specialized object pose estimation to general purpose tracking systems.

For calibration a highly accurate measurement system or an exactly known environment is used to obtain parameters of an individual setup. In robotics the kinematic model of a robot is usually based on engineering data and customized by a calibration procedure to increase the accuracy of the robot [4]. Within a defined workspace the error between desired Cartesian pose and the real pose is measured at multiple positions. Based on this data the model parameters are optimized by error minimization. The measurement system may for example be an optical tracking system that is used to generate a robot signature to compensate for geometrical and flexibility errors in the entire working range [1] of an absolute accurate robot. As the calibration is a offline procedure, it provides no correction of errors which result from flexibilities in the structure of the robot or external influences like deformations based on thermal effects.

There are several concepts of using tracking data online to compensate for errors. Some are based on a high level of knowledge about the shape of the error. In this context the visual feedback can be used to parametrize adaptive controllers [7] [13] [14] to reduce quasi-periodic disturbances. In a medical context movement of organs caused by respiration or the beating heart would belong to this category of disturbances. To achieve the compensation of errors which cannot easily be characterized by an error model, the tracking data is predominantly fed to cascaded controller structures. The Cartesian pose error, measured by a visual sensor, is for instance used as input for an inverse Jacobian controller [2], Cartesian PID controllers or control in feature space [9].

B. Multi sensor object tracking

Sensor fusion is an established technique to improve the quality and reliability of sensor data. Several sensor systems are used to observe a process, and the information from these systems is combined in such a way that it will make use of each individual sensor's strengths and compensate their weaknesses. Often, this is achieved through some variant of the Kalman filter.

A typical example from the field of navigation is the inertial sensors and GPS combination, with an Extended Kalman filter used as the sensor fusion algorithm. An inertial measurement unit can provide frequent measurements of accelerations and angular velocities of a moving object, while the GPS is used to correct, from time to time, the position drift accumulated during integration of the inertial measurements [16] [8]. Sensor fusion has found uses in several other fields as well, for instance motion tracking [11], augmented reality [5] [6] and terrain mapping [15].

For the inertial/GPS combination, the concept of different levels of coupling has been developed. Thus, an inertial/GPS fusion may be loosely, tightly or ultra-tightly coupled, depending on the degree of processing done on the satellite data before it is fed to the sensor fusion algorithm. The less preprocessing, the tighter the coupling. In particular, tightly coupled means that the filter receives each satellite measurement and calculates position, rather than receiving the position calculated by some other method. Similar concepts are used in other areas and for other sensor combinations as well [20] [6]. In [18] the tight coupling concept is transferred to OTS/IMU navigation. Furthermore different sampling rates and latencies of the sensors are explicitly included into the model.

III. Accurate tracking control

In the motion compensation task accuracy is defined with respect to the optical tracking system as that is the reference in the operating room. In that sense the OTS is accurate by definition and the robot is accurate if its pose matches the one of the OTS. The task is to track a certain desired pose ${}^{\mathrm{O}}_{\mathrm{M}}\mathbf{T}_d$ which describes the homogeneous transformation of marker frame M attached to the robot with respect to the object frame O (fig. 3, solid line). The relative pose

$$ {}^{\mathrm{O}}_{\mathrm{M}}\mathbf{T} = {}^{\mathrm{W}}_{\mathrm{O}}\mathbf{T}^{-1} \cdot {}^{\mathrm{W}}_{\mathrm{M}}\mathbf{T} \tag{1} $$

of the robot's marker with respect to the object is given by the robots marker pose and the object pose with respect to the absolute world frame W, which defines the task space (fig. 3, dashed and dotted line, respectively). It is the robot's subtask to track

$$ {}^{\mathrm{W}}_{\mathrm{M}}\mathbf{T}_d = {}^{\mathrm{W}}_{\mathrm{O}}\mathbf{T} \cdot {}^{\mathrm{O}}_{\mathrm{M}}\mathbf{T}_d \tag{2} $$

whereas it is up to the sensor data fusion to provide estimates of ${}^{\mathrm{W}}_{\mathrm{O}}\mathbf{T}$. The desired relative pose ${}^{\mathrm{O}}_{\mathrm{M}}\mathbf{T}_d$ can change over time. It could, e.g. be a whole trajectory generated offline in a planning procedure or simply a constant pose.

In the following section the idea of the proposed task space controller with displacement observer is described for

1 DoF. Afterwards, the error is modeled for a kinematic chain including the robotic setup. The observer feedback is introduced taking the different sampling rates of the MIRO and the OTS into account.

A. Observer Concept

The task requires an accurate robot control. The proposed task space controller is based on an observer feedback. The observer feeds back an error between transformed measurements of internal sensors and measurements of an external sensor. In fig. 2 the idea is shown for a simple 1 DoF system.

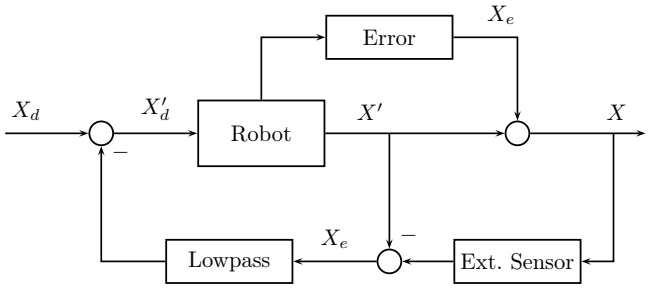

Fig. 2. Observer feedback with an external sensor observing the error of the robot's sensors

The robot here is a position controlled robot, that tracks an desired value X'_d. In the 1 DoF case, the error X_e being a function of the robot's states could, e.g. be a constant offset or an arbitrary function of X'. If it is only a constant offset and therefore not dependent on X', the system in fig. 2 is obviously stable, if the robot as a closed loop system is stable. The position in the task space X will furthermore converge to the desired position X_d, if X' converges to X'_d.

However, in the general case, where X_e is dependent on X' the feedback of X_e can potentially cause stability problems. This is addressed by inserting a lowpass filter to reduce the dynamics of the observer feedback. The complete system can then be divided into two separated systems for the analysis of the stability using the singular perturbation theorem. The error X_e is then considered quasi-constant for the outer loop with the observer. Then the same stability and convergence declarations as above can be applied.

The main difference between the observer feedback compared and a classical cascaded control structure is that the observer compares X with X' which are both measured states, instead of comparing X with X_d. The advantage is that the observer feedback does not reduce the dynamics of the robot controller, because only the observer feedback is reduced in dynamics and not the feedforward path from X_d to X'_d. If the error X_e equals zero, the observer will not have any influence at all, unlike a cascaded controller that reduces the complete dynamics in any case. It is also robust with respect to blackouts of the external sensor, since only the correction can not be updated anymore. The proposed observer feedback aims to preserve the robot's controller performance without adding significant drawbacks.

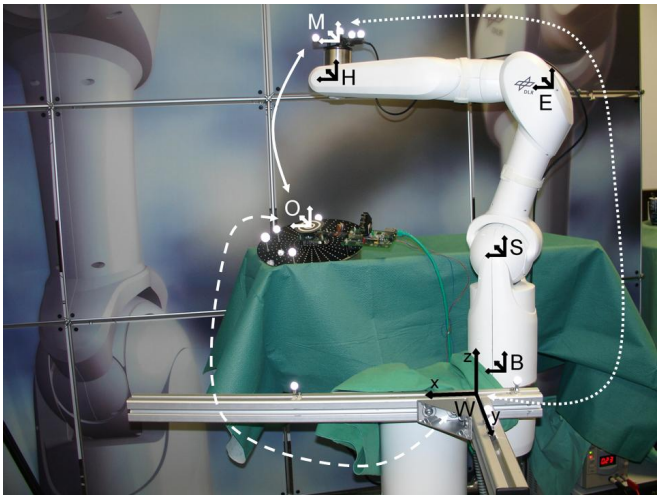

Fig. 3. The transformations of frames in the setup and the MIRO robot are accumulating errors.

B. Error model

The pose of the robot's marker in the world frame is given by the tracking system and a chain of transformations

$$ {}^{\mathrm{W}}_{\mathrm{M}}\mathbf{T} = {}^{\mathrm{W}}_{\mathrm{B}}\mathbf{T} \cdot {}^{\mathrm{B}}_{\mathrm{S}}\mathbf{T} \cdot {}^{\mathrm{S}}_{\mathrm{E}}\mathbf{T} \cdot {}^{\mathrm{E}}_{\mathrm{H}}\mathbf{T} \cdot {}^{\mathrm{H}}_{\mathrm{M}}\mathbf{T} \tag{3} $$

where ${}^{\mathrm{W}}_{\mathrm{B}}\mathbf{T}$ is the location of the robot's base B. The frames ${}^{\mathrm{B}}_{\mathrm{S}}\mathbf{T}$, ${}^{\mathrm{S}}_{\mathrm{E}}\mathbf{T}$ and ${}^{\mathrm{E}}_{\mathrm{H}}\mathbf{T}$ are the frames of the MIRO's shoulder S in base, ellbow E in shoulder and hand H in ellbow frame, respectively. The first transformation combines 3 DoF, the second and third integrate 2 DoF for a coupled joint each. The pose of the marker with respect to the hand is given by ${}^{\mathrm{H}}_{\mathrm{M}}\mathbf{T}$.

Measurements of ${}^{\mathrm{W}}_{\mathrm{M}}\mathbf{T}$ are given by the tracking system and ${}^{\mathrm{B}}_{\mathrm{S}}\mathbf{T}$, ${}^{\mathrm{S}}_{\mathrm{E}}\mathbf{T}$ and ${}^{\mathrm{E}}_{\mathrm{H}}\mathbf{T}$ are calculated by the forward kinematics as functions of link sided joint positions of the MIRO. The frames ${}^{\mathrm{W}}_{\mathrm{B}}\mathbf{T}$ and ${}^{\mathrm{H}}_{\mathrm{M}}\mathbf{T}$ are not directly measured but computed by a numerical optimization from a set of measurements in different kinematic configurations. Due to errors in the transformations, equation (3) is not fulfilled for real data. Taking into account that all terms on the right side of equation (3) contain errors, whereas the left side is considered the ground truth, one can rewrite equation (3) in the form:

$$ {}^{\mathrm{W}}_{\mathrm{M}}\mathbf{T} = {}^{\mathrm{W}}_{\mathrm{B}'}\mathbf{T} \cdot {}^{\mathrm{B}'}_{\mathrm{B}}\mathbf{T} \cdot {}^{\mathrm{B}}_{\mathrm{S}'}\mathbf{T} \cdot {}^{\mathrm{S}'}_{\mathrm{S}}\mathbf{T} \cdot {}^{\mathrm{S}}_{\mathrm{E}'}\mathbf{T} \cdot {}^{\mathrm{E}'}_{\mathrm{E}}\mathbf{T} \cdot {}^{\mathrm{E}}_{\mathrm{H}'}\mathbf{T} \cdot {}^{\mathrm{H}'}_{\mathrm{H}}\mathbf{T} \cdot {}^{\mathrm{H}}_{\mathrm{M}'}\mathbf{T} \cdot {}^{\mathrm{M}'}_{\mathrm{M}}\mathbf{T} \tag{4} $$

In this equation ${}^{\mathrm{W}}_{\mathrm{B}'}\mathbf{T}$, e.g. denotes the transformation that was identified (or measured) and ${}^{\mathrm{B}'}_{\mathrm{B}}\mathbf{T}$ denotes the error associated with it that is needed to get the real transformation ${}^{\mathrm{W}}_{\mathrm{B}}\mathbf{T}$ that we would like to have. However, identifying all error frames needed for correcting and associating them with physical properties such as joint sensor offsets, link lengths and robot base location means calibrating the whole setup in the operating room. This requires a huge set of offline recorded data in different kinematic configurations, especially if flexibility is taken into account.

The approach chosen in this paper is to observe the error online and identify it for the current pose. Unfortunately, the OTS can only measure the ends of the transformation chain

being the markers of the world W and the robot marker frame M. It is not possible to observe how this error is distributed, over ${}^{\mathrm{B}'}_{\mathrm{B}}\mathbf{T}$, ${}^{\mathrm{S}'}_{\mathrm{S}}\mathbf{T}$, ${}^{\mathrm{E}'}_{\mathrm{E}}\mathbf{T}$, ${}^{\mathrm{H}'}_{\mathrm{H}}\mathbf{T}$ and ${}^{\mathrm{M}'}_{\mathrm{M}}\mathbf{T}$. The idea is to choose one of these error transformations and assume all errors to occur there and the other transformations simply to be identity matrices. This arises the question: Which matrix is the most convenient to chose? Concerning the goal of zero steady state error it does not matter because any error matrix can fulfill equation (4) if the others are identity matrices. When taking dynamic motion into consideration this changes. It is then convenient to choose the error matrix which has the smallest gradient, so that it still is approximately correct at the pose the robot is moving to. The smallest gradient has the matrix that is undergoing the fewest motion itself, which is ${}^{\mathrm{B}'}_{\mathrm{B}}\mathbf{T}$.

Neglecting the identity matrices and summarizing the forward kinematics with ${}^{\mathrm{B}}_{\mathrm{H}}\mathbf{T}$ the observed error model is given by:

$$ {}^{\mathrm{W}}_{\mathrm{M}}\mathbf{T} = {}^{\mathrm{W}}_{\mathrm{B}'}\mathbf{T} \cdot {}^{\mathrm{B}'}_{\mathrm{B}}\mathbf{T} \cdot {}^{\mathrm{B}}_{\mathrm{H}}\mathbf{T} \cdot {}^{\mathrm{H}}_{\mathrm{M}}\mathbf{T} \tag{5} $$

C. Observer feedback

Equation (5) only describes the geometric model of the system. Usually, an external measurement system is significantly slower than the robot's internal sensors. This is to be taken into account to ensure data integrity in time.

The optical tracking system provides pose measurements

$$ {}^{\mathrm{W}}_{\mathrm{M}}\mathbf{T}_{\phi(i)} = {}^{\mathrm{W}}_{\mathrm{M}}\mathbf{T}[i] \tag{6} $$

at a discrete step $i \in \mathbb{N}$ of precalibrated marker configurations, where

$$ \phi(i) = i \cdot t_{s,OTS} - t_{l,OTS} \tag{7} $$

maps the measured sample to the physical time. The sampling time and the latency of the OTS are given by $t_{s,OTS}$ and $t_{l,OTS}$, respectively. The measurements of the MIRO robot are the motor positions in joint space $\theta_{\chi(j)}$ and the joint torques $\tau_{\chi(j)}$. The function $\chi(j) = i \cdot t_{s,MIRO}$ associating the j-th sample to the physical time, with the sampling time $t_{s,MIRO}$. The sampling time of the OTS is a multiple of the MIRO and significantly higher.

The link sided positions $\mathbf{q}(\chi(j))$ can be observed

$$ \mathbf{q}_{\chi(j)} = \theta_{\chi(j)} \cdot \mathbf{K}^{-1} \tau_{\chi(j)} \tag{8} $$

with the joint stiffness $\mathbf{K}$. The forward kinematics solution then gives:

$$ {}^{\mathrm{B}}_{\mathrm{H}}\mathbf{T}_{\chi(j)} = fkin(\mathbf{q}_{\chi(j)}) \tag{9} $$

From (5), regarding the different sampling rates, it follows the observation of the correction matrix with one frame corresponding to each measurement of the optical sensor:

$$ {}^{\mathrm{B}'}_{\mathrm{B}}\mathbf{T}_{\phi(i)} = {}^{\mathrm{B}'}_{\mathrm{W}}\mathbf{T} \cdot {}^{\mathrm{W}}_{\mathrm{M}}\mathbf{T}_{\phi(i)} \cdot {}^{\mathrm{M}}_{\mathrm{H}}\mathbf{T} \cdot {}^{\mathrm{H}}_{\mathrm{B}}\mathbf{T}_{\chi(j)} \tag{10} $$

While the above error observations are triggered by incoming data from the OTS the feedback correction frame

$$ {}^{\mathrm{B}'}_{\mathrm{B}}\mathbf{T}^{*}_{\chi(j)} = Lowpass({}^{\mathrm{B}'}_{\mathrm{B}}\mathbf{T}_{\phi(i)}) \tag{11} $$

provides a feedback interpolated in the robot's sampling rate. The lowpass not only reduces the dynamics of the observer feedback to ensure stability but also interpolates the correction matrix and reduces noise.

The desired frame for the robot's inverse kinematics solution is then given by:

$$ {}^{\mathrm{B}}_{\mathrm{H}}\mathbf{T}_{d,\chi(j)} = {}^{\mathrm{B}}_{\mathrm{B}'}\mathbf{T}^{*}_{\chi(j)} \cdot {}^{\mathrm{B}'}_{\mathrm{W}}\mathbf{T} \cdot {}^{\mathrm{W}}_{\mathrm{M}}\mathbf{T}_{d,\chi(j)} \cdot {}^{\mathrm{M}}_{\mathrm{H}}\mathbf{T} \tag{12} $$

The MIRO's position controller implements a controller in joint/motor space taking the joint coupling into account. Motor positions, velocities, joint torques and their derivatives are used in a full state feedback controller [10]. The torque feedback effectively provides vibration damping and an additional disturbance observer reduces motor sided disturbances, such as friction in the joint [17]. The controller is extended with a fifth state, being the integral of the position to ensure convergence to the desired position in the case of link sided disturbances.

IV. Multi sensor object tracking

In [18], we introduced a sensor fusion approach for motion tracking using a combination of inertial sensors and an optical tracking system. The motion of an object is modeled as a process and an extended Kalman filter is used to combine data from the two sensor systems and estimate the states of this process.

$$ \mathbf{x}_{\psi(k)} = ({}^{\mathrm{W}}_{\mathrm{U}}\mathbf{p}_{\psi(k)}, {}^{\mathrm{W}}_{\mathrm{U}}\mathbf{q}_{\psi(k)}, {}^{\mathrm{W}}_{\mathrm{U}}\mathbf{v}_{\psi(k)}, {}^{\mathrm{U}}_{\mathrm{U}}\mathbf{a}_{b,\psi(k)}, {}^{\mathrm{U}}_{\mathrm{U}}\omega_{b,\psi(k)})^{\mathrm{T}} \tag{13} $$

Bias errors of the inertial sensors are expressed with respect to the IMU frame U, which is rigidly connected with the object O frame with ${}^{\mathrm{O}}_{\mathrm{U}}\mathbf{T}$ (U is not shown in fig. 3). As inputs, the process has the acceleration and angular velocity as measured by the IMU:

$$ \mathbf{u}_{\psi(k)} = (\mathbf{a}_{m,\psi(k)}, \omega_{m,\psi(k)})^{\mathrm{T}} \tag{14} $$

where

$$ \psi(k) = k \cdot t_{s,IMU} \tag{15} $$

is a function that associates a discrete time step index k with the continuous time moment when the sample was taken. Note that the IMU and OTS have different sampling rates ($t_{s,IMU}$ and $t_{s,OTS}$ respectively, with $t_{s,IMU} < t_{s,OTS}$). In general an IMU is fast enough so that we can assume its data has no delay. However, the OTS has a significant latency ($t_{l,OTS}$) due to image processing. The OTS measures the outputs of the process, which are the positions of reflective marker balls attached to the object.

$$ \mathbf{y}_{\phi(i)} = ({}^{W}_{\mathrm{M},1}\mathbf{p}_{m,\phi(i)}, {}^{W}_{\mathrm{M},2}\mathbf{p}_{m,\phi(i)}, \cdots, {}^{W}_{\mathrm{M,n}}\mathbf{p}_{m,\phi(i)}) \tag{16} $$

The OTS also provides a quality value between 0 and 1 for each marker. If the quality of a marker measurement is below some threshold, that marker is considered invisible and that measurement not used.

An extended Kalman filter runs in two phases the "predict" and the "correct" phase, which are associated with the process and the measurement model. In our case that means, several "predict" phases will occur between two "correct"

phases, because the sampling time for the IMU is shorter than for the OTS. Furthermore, the latest available OTS measurements are not associated with the latest IMU measurements and therefore the process states, due to latency of the OTS. The IMU measurements and predicted states are stored in a buffer along with the time they were collected/computed at. The correction is not applied to the most recent state estimate but rather to one stored in the buffer, at a time that matches the time of the marker measurements. This way integrity in time is conserved in the sense that only measurements are fused that belong to the same physical time. After each measurement update, the filter runs a series of "predict" steps on the stored states and IMU measurements, to propagate the correction forward to the present. So all available data is used at any time to get good estimates. The increased computational load is no problem since we can assume that enough processing power, like a PC with a CPU, is available.

The kind of sensor fusion employed in our approach is tightly coupled, this means single positions are fed to the Kalman filter instead of pre-computed poses to make use of all visible markers. As long as at least three non-colinear markers are visible the system is completely observable. The filter is able to determine the tracked body's position and orientation as well as all the other states. If only one or two markers are visible during an interval of time (on the order of several seconds [18]), the filter can still use the available information to constrain the states and maintain accuracy in the world frame during this interval. If no markers are visible however the position estimation tends to drift very fast so this situation should be avoided. Another benefit of the IMU/OTS fusion is the increased sample rate, since the sensor fusion algorithm can provide good quality estimates at the rate of the IMU, faster than the rate of the OTS alone. These estimates are also latency compensated and will track the current states without the delays of the OTS.

V. Results

The proposed methods for accurate robot control and object tracking are evaluated in the depicted experiments. The medical light-weight robot MIRO from DLR is combined with the optical tracking system ARTrack2[1]. The tracked object is an experimental platform with 4 markers and one ADIS16350 IMU. A set of precalibrated marker targets is rigidly attached to the robot's tool flange and base. The setup calibration is done by manually adjusting the marker targets with the TCP and base-frame, respectively. The MIRO's communication backbone, a spacewire bus, is running at $3kHz$. The OTS provides data at $60Hz$ and the IMU at $500Hz$.

A. Task space control

The task space controller with observer feedback is implemented as introduced in section III for the 6 DoF task space. The MIRO is initially positioned in the middle of its workspace, as shown in fig. 3. The correction matrix ${}^{B'}_{B}\mathbf{T}$ is initially the identity matrix[2]. The lowpass is implemented as a first order filter with a cutoff frequency of $0.5Hz$ which caused no stability problems. Responses to interpolated position commands along the y-axis in the task space were evaluated. In fig. 4 a slow trajectory with $0.01\frac{m}{s}$ is shown in the upper graphs and a fast trajectory with $0.1\frac{m}{s}$ in the lower ones. The right side illustrates enlargements of the convergence zones, around $10sec$ and $1sec$, respectively.

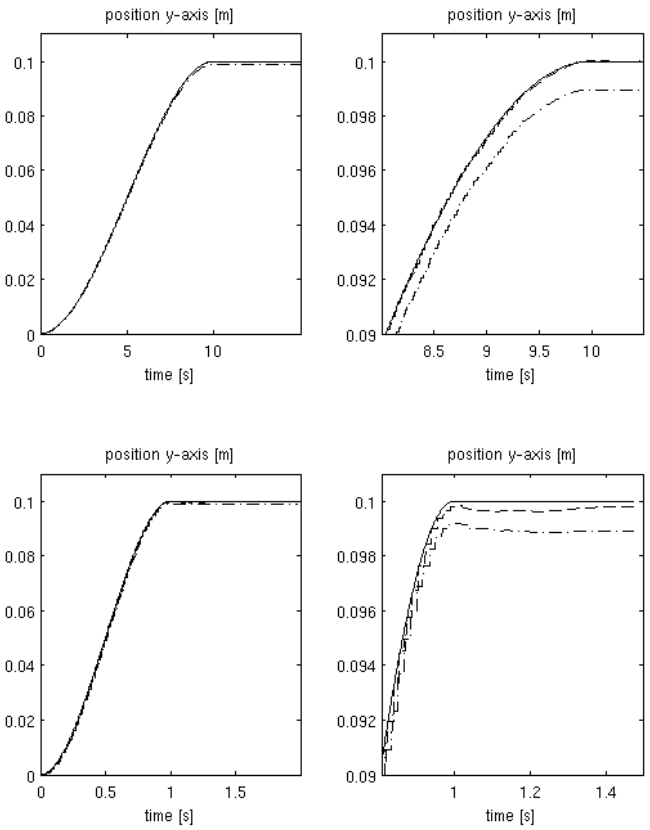

Fig. 4. Response to an interpolated position command in the y-axis; slow $0.01\frac{m}{s}$ on the top and fast $0.1\frac{m}{s}$ on the bottom; desired trajectory (solid), control without observer (dash-dotted), control with observer (dashed)

The MIRO tracks the desired position (solid line) in the task space with an increasing error showing a slow drift away from the track, if no observer is used (dash-dotted line). The remaining steady state error is about $1mm$ for $100mm$ motion. However, with the observer (dashed line) the error practically converges to zero or below $0.1mm$ which is within the magnitude of the sensor noise. For the slow motion on top of fig. 4 the MIRO perfectly tracks the desired trajectory. The fast motion on the bottom shows the limitations of the approach. The controller with observer still performs better than the controller without observer at any time. It drifts a little bit due to the reduced dynamics of the observer feedback and finally converges $0.6sec$ after the reference trajectory stops.

The plots in fig. 5 correspond to the response to the in-

[1] 2009-09 url:http://www.ar-tracking.de/ARTtrack2.52.0.html

[2] The base frame is rotated 17° around the z-axis with respect to the world frame.

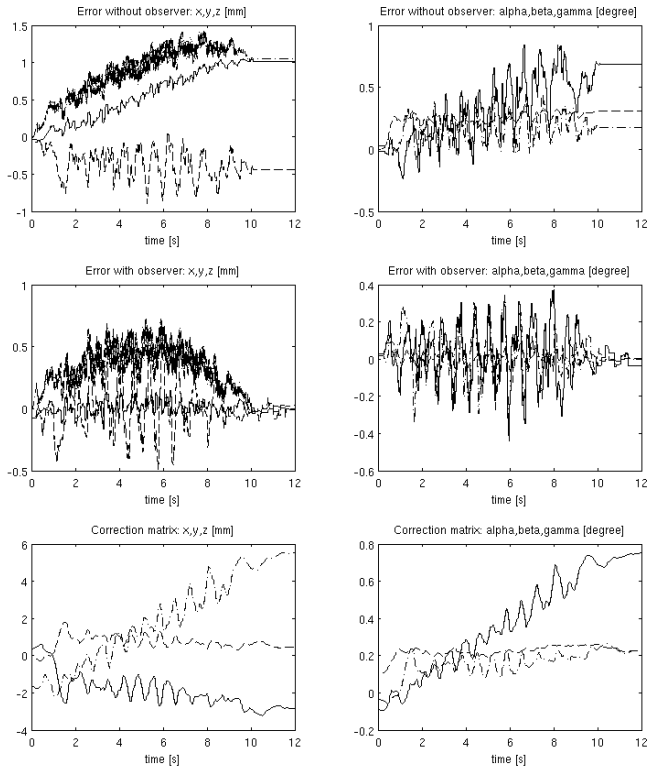

Fig. 5. Responce to an interpolated position command in the y-axis with $0.01\frac{m}{s}$; Translations (left column) with x (solid), y (dash-dotted), z (dashed) and Orientation (right column) around x (solid), y (dash-dotted), z (dashed); Position and Orientation error without observer (top row) and with observer (middle); Bottom row shows the correction matrix

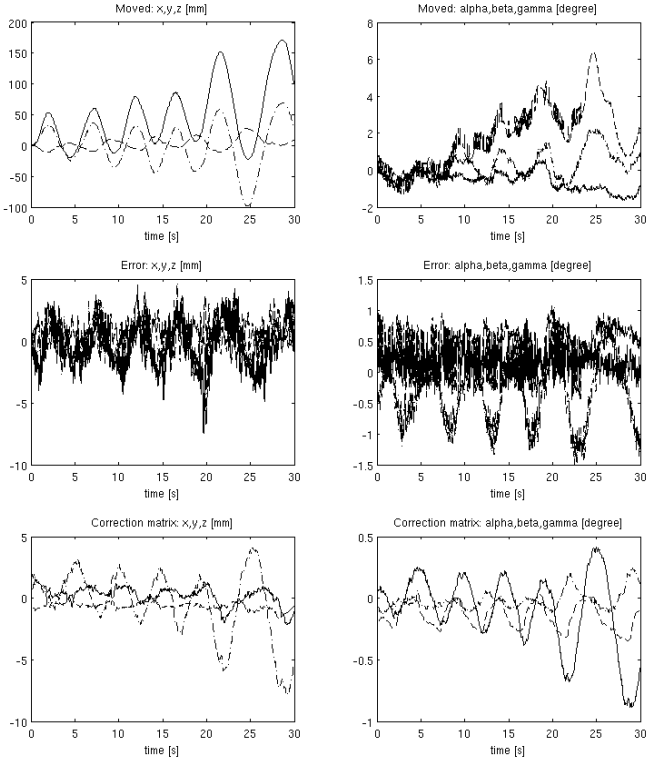

Fig. 6. Free motion of the handheld object platform in 6 DoF; Translations (left column) with x (solid), y (dash-dotted), z (dashed) and Orientation (right column) around x (solid), y (dash-dotted), z (dashed); Motion from initial pose (top row); Error of a virtual tool acting on the object (middle); Plots on the bottom show the correction matrix

terpolated position command with $0.01\frac{m}{s}$ motion. The errors for position (left) and orientation (right) for the controller without observer are shown on top, where small errors occur in all 6 DoF of the task space. When the observer is used, these errors converge to zero. On the left a phase lag of the controller can be seen in the y-axis (dash-dotted line). On the bottom line the correction matrix ${}^{\mathrm{B'}}_{\mathrm{B}}\mathbf{T}$ that absorbs the error is shown.

B. Motion Compensation

Experiments were done with the complete system evaluating the task space control and the object tracking in combination. The pose estimates of the target platform provided by the sensor data fusion were additionally filtered with a $10Hz$ first order lowpass filter. Even though the sensor data fusion reduces noise [18] compared to the OTS alone, the quick responding controller of the MIRO requires an additional smoothing of the commanded pose. The desired relative pose ${}^{\mathrm{O}}_{\mathrm{M}}\mathbf{T}_d$ is considered to be a virtual tool attached to the robot with it's distal end[3] effecting the target object. The target object pose ${}^{\mathrm{W}}_{\mathrm{O}}\mathbf{T}$ is therefore independently measured with the OTS and compared to ${}^{\mathrm{W}}_{\mathrm{M}}\mathbf{T} \cdot {}^{\mathrm{O}}_{\mathrm{M}}\mathbf{T}_d^{-1}$.

The plots on top of fig. 6 show the motion of the object platform with respect to an initial pose of the object that is to be compensated. The platform is moved in translation (top left) with a magnitude from about $50mm$ to over $150mm$ on the dominant x-axis (solid). The error (middle left) is below $5mm$ and is dominated by the phase lag of the estimated and filtered pose, as well as the lag of the robot's position controller. The magnitude of the correction matrix (bottom left), as expected, increases with the magnitude of motion. The error in orientation (middle right) stays within the range of ± 1 degree, for the complex motion. The magnitudes of the correction matrix in translation and orientation ${}^{\mathrm{B'}}_{\mathrm{B}}\mathbf{T}$ (bottom row) correspond to the magnitude of the motion.

[3]This is illustrated with a laser pointer in the video attachment.

VI. Conclusion and Future Work

The task of tracking an object with a robot was divided into two subtasks. The first is to control the robot accurately in the task space and the other one is tracking the moving object. The task space was defined by an optical tracking system locating the robot and the moving object with markers, in a typical medical scenario. The robot's position controller was enhanced by an observer comparing the position measurements of the robot and of the optical tracking system. In the robotic setup the observer feedback efficiently compensates for residual errors predicated on robotic setup errors as well as kinematic errors. In addition the observer preserves the high dynamics of the MIRO's position controller and enhances the robot with absolute accuracy. An extended Kalman filter fuses measurements of an inertial measurement unit and optical data. It provides

pose estimates with reduced latency and noise compared to stand-alone optical tracking. It furthermore increases the robustness to marker occlusions. Tracking of a constant relative pose of the MIRO robot with respect to the freely moving object was shown in the 6 DoF task space.

Application of the proposed structure will be compensation of respiration motion in, e.g. laser osteotomy or spinal surgery. Future versions might also be adapted to beating heart motion compensation with an endoscope serving as external sensor. Tracking performance could be improved by more sophisticated error modeling. Instead of assuming all errors to occur in one frame of the transformation chain it could be distributed. Application specific reductions of DoF of the task space and assumptions about periodicity of physiological motion can be used to further reduce the residual tracking error.

REFERENCES

[1] Metris k600 measurement systems calibrate the absolute accurate robots at kuka, 09 2009.

[2] R.A. Beasley, R.D. Howe, and P.E. Dupont. Kinematic error correction for minimally invasive surgical robots. In *Robotics and Automation, 2004. Proceedings. ICRA '04. 2004 IEEE International Conference on*, volume 1, pages 358–364 Vol.1, April-1 May 2004.

[3] Goo Bong Chung, Soo Gang Lee, Sungmin Kim, Byung-Ju Yi, Whee-Kuk Kim, Se Min Oh, Young Soo Kim, Jong Il Park, and Seong Hoon Oh. A Robot-Assisted Surgery System for Spinal Fusion. In *Proceedings of the 2005 IEEE/RSJ International Conference on Intelligent Robots and Systems*.

[4] A.Y. Elatta, Fan Liang Zhi, Li Pei Gen, Luo Fei, and Yu Daoyuan. An overview of robot calibration. *Information Technology Journal*, 3(1):74–78, 2004.

[5] Eric Foxlin. Head-tracking relative to a moving vehicle or simulator platform using differential inertial sensors. In *Proceedings of SPIE*, volume Volume 4021: Helmet- and Head-Mounted Displays V, pages 133–144, April 2000.

[6] Eric Foxlin, Michael Harrington, and George Pfeifer. Constellation: A wide-range wireless motion-tracking system for augmented reality and virtual set applications. In *Proceedings of SIGGRAPH*, pages 371–378, 1998.

[7] T.J. Franke, O. Bebek, and M.C. Cavusoglu. Prediction of heartbeat motion with a generalized adaptive filter. In *Robotics and Automation, 2008. ICRA 2008. IEEE International Conference on*, pages 2916–2921, May 2008.

[8] Michael George and Salah Sukkarieh. Tightly Coupled INS/GPS with Bias Estimation for UAV Applications. In *Proceedings of Australiasian Conference on Robotics and Automation (ACRA)*, December 2005.

[9] Paolo Robuffo Giordano, Andreas Stemmer, Klaus Arbter, and Alin Albu-Schäffer. Robotic assembly of complex planar parts: An experimental evaluation. In *IROS*, pages 3775–3782, 2008.

[10] L. Le-Tien, A. Albu-Schäffer, and G. Hirzinger. MIMO state feedback controller for a flexible joint robot with strong joint coupling. In *Proceedings of the IEEE International Conference on Robotics and Automation (ICRA)*, pages 3824–30, Roma, Italy, April 2007. DOI: 10.1109/ROBOT.2007.364065.

[11] Joo Lus Marins, Xiaoping Yun, Eric R. Bachmann, Robert B. McGhee, and Michael J. Zyda. An Extended Kalman Filter for Quaternion-Based Orientation Estimation Using MARG Sensors. In *Proceedings of the 2001 IEEE/RSJ International Conference on Intelligent Robots and Systems*, pages 2003–2011, October-November 2001.

[12] Tobias Ortmaier, Holger Weiß, Ulrich Hagn, Matthias Nickl, Alin Albu-Schäffer, Christian Ott, Stefan Jörg, Rainer Konietschke, Luc Le-Tien, and Gerd Hirzinger. A Hands-On-Robot for Accurate Placement of Pedicle Screws. In *Proceedings of the 2006 IEEE International Conference on Robotics and Automation*, 2006.

[13] C.N. Riviere, J. Gangloff, and M. de Mathelin. Robotic compensation of biological motion to enhance surgical accuracy. *Proceedings of the IEEE*, 94(9):1705–1716, Sept. 2006.

[14] C.N. Riviere, A. Thakral, I.I. Iordachita, G. Mitroi, and D. Stoianovici. Predicting respiratory motion for active canceling during percutaneous needle insertion. In *Engineering in Medicine and Biology Society, 2001. Proceedings of the 23rd Annual International Conference of the IEEE*, volume 4, pages 3477–3480 vol.4, 2001.

[15] M. Sartori, M. Starek, and K. C. Slatton. Alsm data processing. Technical Report REP_2004-06-001, Geosensing Engineering and Mapping, Civil and Coastal Engineering Department of the University of Florida, June 2004.

[16] Salah Sukkarieh, Eduardo M. Nebot, and Hugh F. Durrant-White. Achieving Integrity in an INS/GPS Navigation Loop for Autonomous Land Vehicle Applications. In *Proceedings of IEEE Conference on Robotics and Automation*, May 1998.

[17] Luc Le Tien, Alin Albu-Schäffer, Alessandro De Luca, and Gerd Hirzinger. Friction observer and compensation for control of robots with joint torque measurement. In *IROS*, pages 3789–3795, 2008.

[18] Andreas Tobergte, Mihai Pomarlan, and Gerd Hirzinger. Robust multi sensor pose estimation for medical applications. In *Proceedings of the 2009 IEEE/RSJ International Conference on Intelligent Robots and Systems*, pages 492–497, 2009.

[19] Hagn U., Nickl M., Jörg S., Passig G., Bahls T., Nothhelfer A., Hacker F., Le-Tien L., Albu-Schffer A., Konietschke R., Grebenstein M., Warpup R., Haslinger R., Frommberger M., and Hirzinger G. The DLR MIRO: A versatile lightweight robot for surgical applications. In *Industrial Robot: An International Journal2008*.

[20] Gregory Francis Welch. *SCAAT: Incremental Tracking with Incomplete Information*. PhD thesis, Department of Computer Science, University of North Carolina at Chapel Hill, October 1996.